Vol. 40, No. 3 (2018) 488-500, DOI: 10.24874/ti.2018.40.03.14

Tribology in Industry

www.tribology.rs

RESEARCH

Tribological and Electrochemical Properties of AISI D3 Steel Coated with Hafnium Carbon Nitride

W. Piedrahita[a], J.C. Caicedo[a], W. Aperador[b]

[a] *Tribology, Polymers, Powder Metallurgy and Processing of Solid Recycled Research Group, Universidad del Valle, Cali, Colombia,*
[b] *School of Engineering, Universidad Militar Nueva Granada, Bogotá-Colombia.*

Keywords:

HfCN coatings
Corrosion resistance
Wear resistance
Industrial applications

Corresponding author:

Julio Caicedo Angulo
Department of Materials Engineering, Universidad del Valle Universidad del Valle, Cali, Colombia.
E-mail: g.ing.materiales@gmail.com

A B S T R A C T

In this research work, hafnium carbonitride (HfCN) coatings were developed via physical vapor deposition with the aim to determine the electrochemical behavior of the HfCN layers on industrial steel substrates. The HfCN coatings, deposited at various negative bias voltage were characterized by X-ray diffraction (XRD), exhibiting the crystallography orientations corresponding to a mix of HfCN, HfC and HfN phases, while the X-ray photoelectron spectroscopy (XPS) measurements were used to determinate the chemical composition of the carbon nitride coatings. By using electrochemical impedance spectroscopy (EIS) and Tafel curves, it was possible to estimate the electrochemical behavior of the HfCN coatings in a sodium chloride (NaCl) solution. Moreover, scanning electron microscopy (SEM) was performed to analyze morphological and chemical surface changes on the HfCN layer due to the reaction in NaCl/HfCN/steel surface interface. The electrochemical behavior of the HfCN coatings in relation to the uncoated AISI D3 steel showed a reduction of 98 % in corrosion rate, indicating that the applied HfCN coatings may be a promising material for industrial applications.

1. INTRODUCTION

The evolutions in many materials such as nitrides and carbides have presented interesting results, producing novel ternary materials (CrCN, BCN, TiCN,) [1-3] and novel interactive systems (TiAlCN/HfCN, TiCN/TiNbCN) [4,5]. Novel interactive materials can be developed because the transition metal compounds, forming carbides and nitrides, deposited as thin coatings on metallic substrates have been widely investigated and used in industrial applications due to their remarkable mechanical and functional properties [6]. However, industrial devices are exposed to various aggressive media, including corrosive attack; therefore, there is a growing need to produce electrochemical protection systems to preserve the surface integrity. The coatings based on oxides, carbides, nitrides and borides, may provide alternative solutions due to their high chemical stability [1,7]. In this sense, hafnium carbonitride (HfCN) is a material produced by a conjugate complex of hafnium carbide (HfC) and hafnium nitride

(HfN), which shows a strong interaction between carbon (C), nitrogen (N) and hafnium (Hf), generating strongly coordinated covalent bonds, similar to TiCN and BCN materials. In the literature, few reports have been found for HfCN materials, in terms of crystal structure and a stoichiometric ratio. G. Kamath et al. [8] presented the possibility to produce HfCN coatings via physical vapor deposition (PVD) technique with high thermodynamic stability. However, the literature presents few researches focused on studying the nitride corrosive-erosive behavior. This corrosive-erosive behavior on steel coated with ZrCN coatings has been studied and reported by C. M. Cotruta et al. [7]. In their study, the authors found that coated substrates showed a better erosion resistance under electrochemical attack, and subsequently, the coatings were removed from the substrate surface by surface corrosion [7]. The aim of this work is to study the effect of negative bias voltage on the mechanical, tribological and corrosion resistance of commercial AISI D3 steel uncoated, and AISI D3 steel coated with HfCN layers deposited with different bias voltages from 0 V to -150 V under corrosive environment containing chloride ions (Cl^-).

2. EXPERIMENTAL SECTION

In this research, HfCN coatings have been grown on Si (100) and AISI D3 steel substrates (chemical composition: C= 2.1, Mn=0.6, Si= 0.6, Cr= 12.2, Ni= 0.30, W=1.0, V= 1.0, P= 0.03, S=0.03, Cu= 0.25 and Fe=92.8) by using a multitarget magnetron reactive sputtering technique, with an r.f. source (13.56 MHz) and two hafnium (Hf) and graphite (C) targets with purity at 99.9 % for both targets. The deposition parameters for obtaining high-quality coatings were: sputtering power of 450 W for Hf and 400 W for the C target; substrate temperature of 300 °C; under circular rotation substrate with 60 RPM to facilitate the formation of the stoichiometric coating; the sputtering gas was a mixture of Ar 92.5 % (50 sccm) and N_2 7.5 % (3.75 sccm) with a total working pressure of 6×10^{-3} mbar. An unbalanced r.f. bias voltage was applied, which generated a negative signal of 0 V, -50 V, -100 V and -150 V to systematically study its effect on the electrochemical properties of the coatings. The total thickness of all the coatings was kept constant around 1.5 μm. The crystallography structure was analyzed via X-ray diffraction (XRD), with a Bruker D8 Advance diffractometer with copper anode X-ray tube (Cu-Kα radiation with λ = 1.5405 Å) operating at 45 kV and 40 mA and scintillation detector using the θ-2θ setting performing a sweep from 20° to 80° with a step of 0.01° and a step time of 2 s. The chemical composition of the coatings was determined by energy dispersive X-ray (EDX) analysis using a Philips XL 30 FEG and X-ray photoelectron spectroscopy (XPS) in a SPECS Sage HR 100 spectrometer with a non-monochromatic X ray source (Al Kα anode of 1486.6 eV energy and a power applied of 300 W and calibrated using the $3d_{5/2}$ line of Ag with a full width at half maximum (FWHM) of 1.1 eV). The selected resolution for the spectra was 30 eV of pass energy and 0.5 eV/step for the general survey spectra, 10 eV of Pass Energy and 0.15 eV/step for the individual spectra of the different elements. All measurements were made in an ultra-high vacuum (UHV) chamber at a pressure around 1×10^{-3} mbar. Samples were etched for 5 min with an Ar^+ ion beam with energy of 3 keV. The pressure of chamber during etching was set around 5×10^{-9} mbar.

Morphological properties in anodized magnesium were studied by scanning electron microcopy (SEM) in a JSM 6490LV JEOL microscope. The thickness for ternary coatings was 1.5 ±0.1 μm, and was determined by means of a (Dektak 3030) profilometer. Electrochemical Impedance Spectroscopy (EIS) and Tafel polarization curves were obtained at room temperature (25°C) in static conditions (without aeration), using a cell with a working electrode of an exposed area of 1 cm^2, an Ag/AgCl (3.33 M KCl) reference electrode and a platinum wire counter-electrode under a 3.5% NaCl solution. For EIS results, the frequency sweeps were conducted in the range from 100 kHz to 0.001 Hz using sinusoidal signal amplitude of 10 mV applied to the working electrode (sample) and reference electrode. Diagrams for Tafel polarization curves were obtained at a sweep speed of 0.125 mV/s in a voltage range from 0.25 to 0.25 V vs Ag/AgCl. This voltage range was defined with respect to the open circuit potential (OCP). These curves allow finding anodic and cathodic slope values in each case, which are necessary to calculate a correct value of the corrosion rate for all systems. The parameter, i_{corr}, can be used to

calculate the average corrosion rate, which represents the general corrosion resistance. Prior to beginning the polarization curves procedures, the samples were submerged in a 3.5 % NaCl solution for 30 min in order to establish the free corrosion potential values (E_{corr}) at which the polarization curves measurements were initiated, to identify the surface corrosion process on AISI D3 steel coated with HfCN layers, SEM images and EDX analysis were performed. Finally, mechanical and tribological properties were carried out by using the nanoindenter (UBI1-Hysitron) under load and unload mode with a matrix measurements of 25 points and maximum load of 9 mN. Tribological characterization was done by means of Microtest, MT 400-98 tribometer, using a 6mm diameter 100Cr6 steel ball like pattern slide. The tribological tests (Pin On disc and scratch test) were carried out under a closed friction system with applied load of (50 N), the room temperature was (25 °C), low relative humidity was (20 %), without lubricant presence, the metallic counterpart (100Cr6) was used with the aims to simulate the industrial behavior when cutting tools coated with HfCN coatings works under industrial conditions.

3. RESULTS

3.1 X-ray diffraction

Figure 1 shows the XRD patterns of the HfCN coatings deposited on Si (100) for different r.f. negative bias voltages from 0 V to -150 V. The XRD patterns indicate that the coatings have a cubic structure based on complex conjugate with two substructures of hafnium carbide (HfC) and hafnium nitride (HfN). The strongest peaks correspond to the HfCN (111), and (220) planes of the FCC structure. The lattice parameters, (a_0) for the different coatings were obtained from the Nelson-Riley function, listed in Table 1 and Table 2. The presence of the HfCN (111) is associated with a substitution mechanism, where C atoms replace N atoms, resulting in a Hf-ordered C–N disordered FCC NaCl-type structure in which Hf is placed in the Wyckoff site 4a, while C and N atoms occupied randomly the Wyckoff site 4b [3, 6]. This means that the nitrogen gas flow rate directly influences the structure of the Hf-C-N coatings. When the nitrogen gas flow rate is around 16 sccm and r.f. negative bias voltages from 0 V to -150 V are used, Hf access to the deposition surface is facilitated; hence, the FCC structure is determined by a partially ordered structure with Hf atoms, creating vacancies in non-metallic sublattices [3, 6]. For higher negative bias voltage (−150 V), an abrupt change in HfCN (111) peak position was observed, presenting a residual stress increase due to the movement of this peak toward higher angles compared to other single layer. The stress changes in HfCN (111) peak position came together with a low symmetric broadening and a decrease in its intensity.

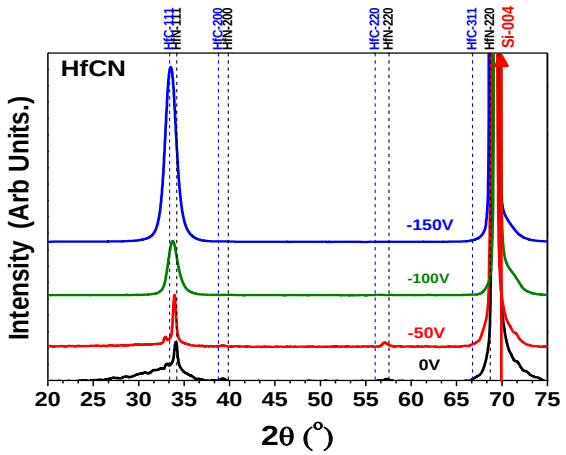

Fig. 1. XRD patterns for the HfCN coatings grown with different r.f. negative bias voltages from 0 to -150 V. Dashed lines indicate the position of the peaks obtained from JCPDF files ((HfN) JCPDF 00-00-06-0516 and (HfC) JCDDF 00-00-06-0510.

In this research the polycrystalline HfCN coating was observed, in this sense the texture coefficient (Tc) was analyzed according to:

$$Tc_{(hkl)} = \frac{\frac{I_{(hkl)}}{I^0_{(hkl)}}}{\frac{1}{N}\sum_{i=1}^{N}\frac{I_{(hkl)}}{I^0_{(hkl)}}} \quad (1)$$

where I(hkl) is the relative intensity measurement plane (hkl), I_0(hkl) is the intensity standard JCPDS files taken of the different planes and N data is the number of planes present in the spectrum. According to this method, a greater (high) value of texture coefficient for a particular crystallographic plane indicates that a preferential orientation exists for this crystallographic plane within the analyzed sample [11]. Therefore, from Table 1 it is possible to analyze a weak texture coefficient due to that all intensities for all peaks are very similar.

Table 1. Texture coefficient value of coatings type Hf-C-N.

Plane	$TC_{(hkl)}$ $HfCN_{0V}$	$TC_{(hkl)}$ HfCN -50V	$TC_{(hkl)}$ HfCN -100V	$TC_{(hkl)}$ HfCN -150V
(111)	0.9	1.1	1.3	1.5

3.2 X-Ray photoelectron spectroscopy

The XPS survey spectra for all Hf-C-N coatings as a function of the negative bias voltage from 0 V to -150 V are shown in Fig. 2. The chemical compositions of all samples are listed in Table 2. It was found that the negative bias voltage and the Hf/(C+N) ratio was around 0.6 for all samples. The samples showed low oxygen presence that can be attributed to the high affinity of metals for oxygen, observing thus oxygen contribution evidenced in the survey spectra. Therefore, also the oxygen presence may be due to low residual oxygen within the deposition system.

Table 2. Lattice parameter and chemical compositions determined from the XPS analysis.

Negative bias voltage (V)	a_0 (nm) FCC (111)	Hf (at.%)	C (at.%)	N (at.%)	Hf-C carbide (%)
0	0.4559	53.7	19.5	26.8	2.7
50	0.4570	57.2	18.3	25.4	2.9
100	0.4610	57.0	20.0	23.0	3.3
150	0.4627	51.6	27.5	20.9	3.7

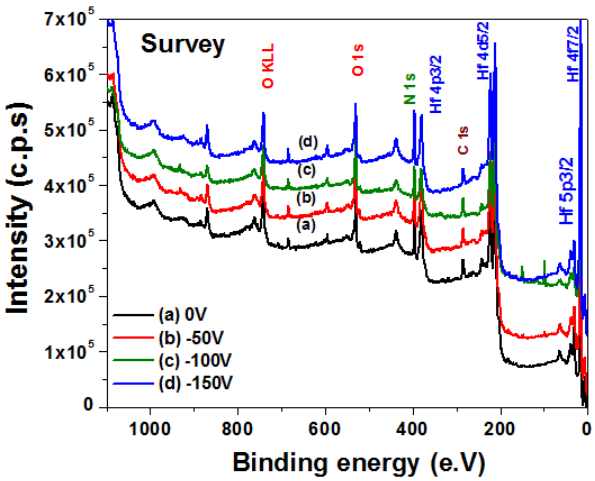

Fig. 2. XPS survey spectra for all the Hf-C-N coatings as function of the r.f negative bias voltage.

The high-resolution C 1s core level spectra for the Hf–C–N coatings are shown in Fig. 3. The fitting of the C 1s spectra showed the presence of two main components, one attributed to C-C bonds at around 285.2 eV [8-10] and another attributed to Hf-C bonds at around 281.46 eV [12]. From the analysis of the fitting, it was found that the amount of Hf-C carbide bonds increased with the negative bias voltage (Table 2) indicating that the bias voltage favors the formation of these bonds [12,13]. In the C 1s spectra, other minor components were found which could be attributed to C-N around 287.56 eV [12,14-17].

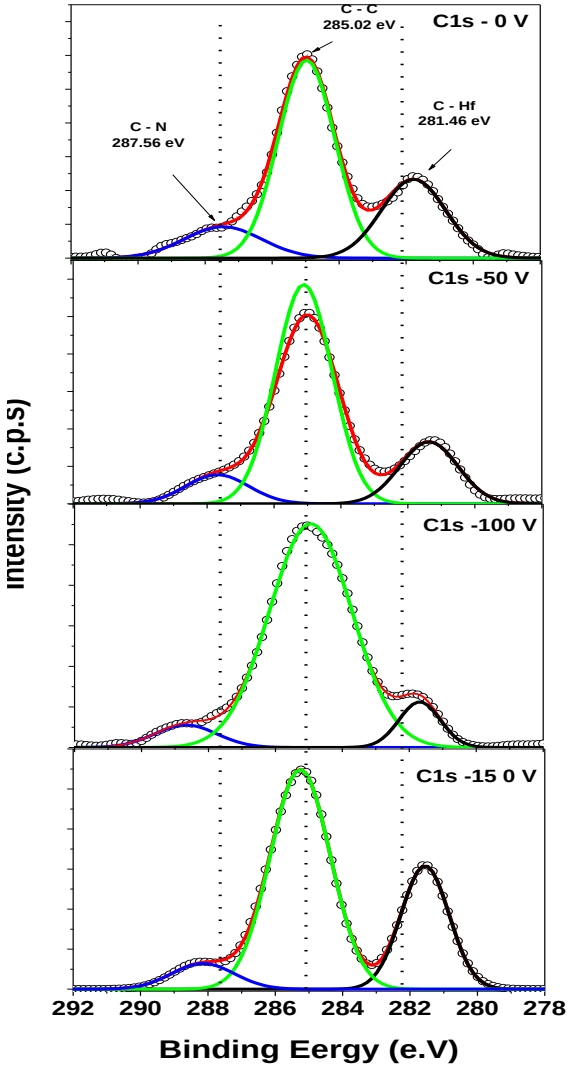

Fig. 3. High-resolution C 1s spectra for the Hf-C-N coatings as function of applied negative bias voltage.

3.3 X- Scanning Electron Microscopy (SEM) Analysis

Figure 4 shows the SEM micrograph for all HfCN coatings surface before the tribological and electrochemical experiments. In these SEM micrographs, it is possible to observe the surface morphology of the Hf-C-N coatings as a function of applied negative bias voltage. Moreover, the cross section shows the transversal growth associated to the Hf–C–N coating with applied

bias voltages. The images show homogeneous surfaces without cracks or delamination generated during the deposition process. The chemical compositions were also analyzed by XPS results. In this sense, the SEM micrograph denotes the difference in the atomic weight of the molecules in the material surface and the influence of them in the gray scale in the micrograph [18].

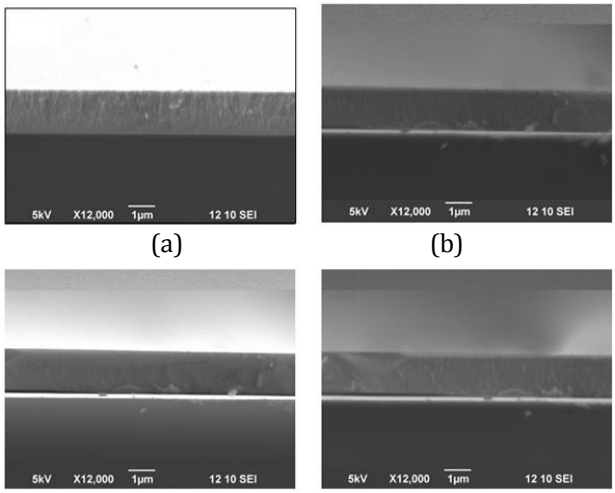

Fig. 4. SEM Micrograph for HfCN coatings deposited with different applied negative bias voltage: (a) 0 V, (b) -50 V, (c) -100 V and (d) -150 V.

3.4 Electrochemical impedance spectroscopy (EIS) and Tafel polarization curves

The electrochemical properties studied with the Nyquist diagram are shown in Fig. 5 for the imaginary part of the impedance versus its real part, for all the Hf-C-N coatings grown at different negative bias voltage: 0 V (filled circle symbol), -50 V (red inverted triangles), -100 V (green filled stars), -150 V (filled black triangles) and for the uncoated AISI D3 steel substrate (filled black square). A strong dependency with the applied r.f. negative bias voltage was observed. From Z´(Z´´ = 0) to Z´(Z´´max) for the intercept of the curve with the X axis Z´(Z´´max), after the experimental data fit, the system provides a Randles cell equivalent circuit (Fig. 6) [19,20], simulating the substrate coating and coating-electrolyte interfaces, as a double layer capacitance in parallel with the Hf-C-N coating resistance and the electrolyte resistance (NaCl), due to the reaction ion transfer [21] from the electrolyte to the metallic substrate. The values for the polarization resistance (Rp) were extracted from the Nyquist diagrams and the equivalent circuit (Fig. 6). Results, listed in Fig. 8 part a, indicate that polarization resistance decreases when the applied negative bias voltage increases. In any case, the polarization resistance for the ternary coatings is bigger than that for the uncoated steel substrate (AISI D3).

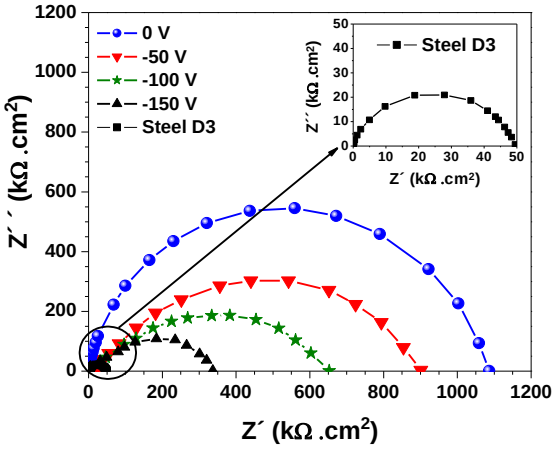

Fig. 5. Impedance diagrams of (a) HfCN coatings deposited on AISI D3 steel substrate with applied bias voltages from 0 V to -150 V, included uncoated steel D3.

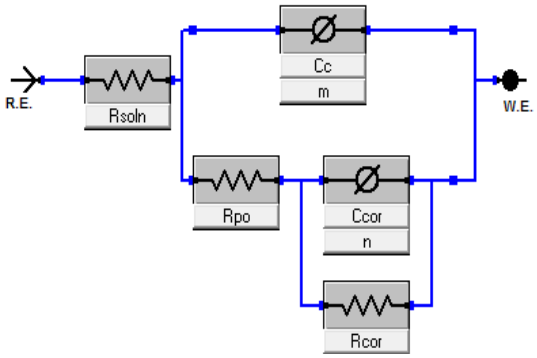

Fig. 6. Equivalent circuit used for simulation of the experimental data of the HfCN coatings. Reference electrode (RE), electrolyte resistance (Rsoln), polarization resistance (R_{corr}) (coatings), coating capacitance (C_{corr}), and working electrode (WE).

The Randles cell equivalent circuit shows the theoretical simulations of the total impedance values (Fig. 6). In this case, the substrate has only one inflection and this effect is due to the oxide layer that is formed from the contact of the steel with the aggressive solution (NaCl) to which it is subjected. The total impedance data, best known as the sum of the resistances $R_{po}+R_{cor}$, decrease with the increase of applied negative bias voltage. It is observed in this study that the values of ($R_{po}+R_{corr}$) are much higher than those found in the substrate because the electrolyte is very aggressive and generates a higher reaction rate on the uncoated steel. So, the circuit presented in

Fig. 6 can be explained as R_s = solution resistance, Rpo = resistance polarization (coating + steel), R_{corr} = polarization resistance (steel), C_c = double layer capacitance (coating + steel), C_{corr} = double layer capacitance (steel).

Tafel polarization curves and the corrosion potential as a function of the corrosion current density for the HfCN coating can be observed in Fig. 7. Tafel polarization curves have been used to calculate the surface corrosion rate. Tafel polarization results are also strongly dependent on the applied bias voltage to the HfCN coatings, indicating the influence of the growth parameters, on the corrosion properties. The curves for the HfCN coatings are in the negative region of the corrosion potential, indicating that in any case there is an ion transfer from electrolyte to the metallic substrate. The slopes of the anodic and cathodic zone, and also the plateau region of the Tafel curves can give information about the electrochemical properties such as corrosion rate. The plateau value increases strongly for the coating at zero bias voltage in comparison to that value from the uncoated substrate. However, when the negative bias voltage is increased, the protection decreases nearing the nature of the bare substrate [22-24]. The sample deposited at a negative bias of -150 V showed the higher susceptibility to HfCN corrosion. This is probably due to the porosity of the coating produced by the ion bombardment at high bias voltages [22]. However, the passivized coatings generate a protective layer that responds better to corrosive events than the uncoated AISI D3 steel substrate.

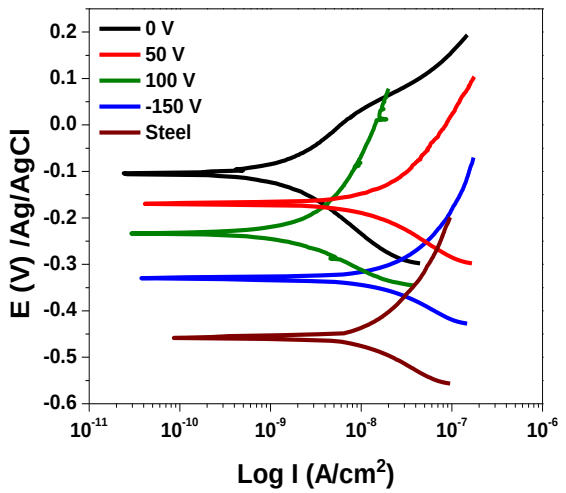

Fig. 7. Tafel curves of Hf-C-N, coatings grown on AISI D3 steel substrate with applied bias voltages from 0 V to -150 V.

Figure 8 shows the electrochemical properties of the Hf-C-N coatings, moreover the uncoated AISI D3 steel substrate presents the highest corrosion resistance compared to the HfCN/steel (D3) system. Figure 8a shows a clear trend of the polarization resistance (R_p) as a function of the applied negative bias voltage. Fig. 8b shows the corrosion rate (Vc) as a function of the negative bias voltage. When analyzed, the AISI D3 steel coated with HfCN deposited at -150 V presented the lowest R_p due to that a higher applied bias voltage can induce residual stress and micro-pores, which can affect the coating integrity generating thus a reduction in the electrochemical protection (Fig. 5).

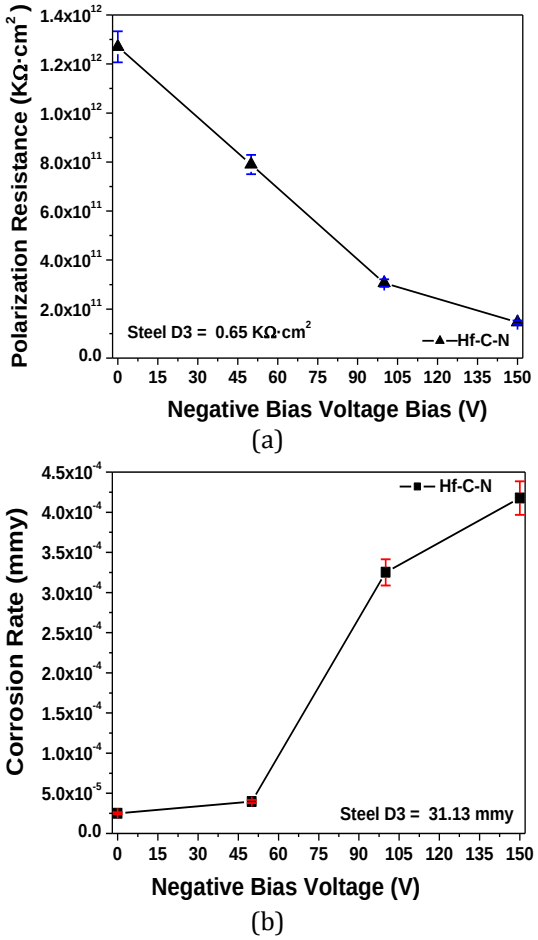

Fig. 8. Electrochemical properties for Hf-C-N coatings: (a) polarization resistance as a function of applied negative bias voltage, and (b) corrosion rate as a function applied negative bias voltage.

Moreover, the corrosion rate (Vc) showed a dramatic increase for the uncoated steel substrate, which differs for Hf-C-N/steel (D3) deposited with 0 V where it is possible to find a reduction in the lower corrosion rate. Also, coatings deposited with different negative bias

voltages present changes in the corrosion rate, therefore, exhibiting more (Vc), compared to all other Hf-C-N coatings shown in this work. This effect can be due to the possibility for ions (Cl^-) to easily migrate from the coating surface to the steel surface through the micro-pores generated by the bombarding Ar^+ atoms when the bias voltage is -150 V.

3.5 Surface analysis after corrosive attack

After the Tafel corrosion test, the SEM micrographs (Fig. 9) were acquired in order to observe the different areas exposed in the corroded systems Hf-C-N. From SEM micrographs, it was possible to identify the corrosion zones for the coating deposited with 0 V (Fig. 9a).

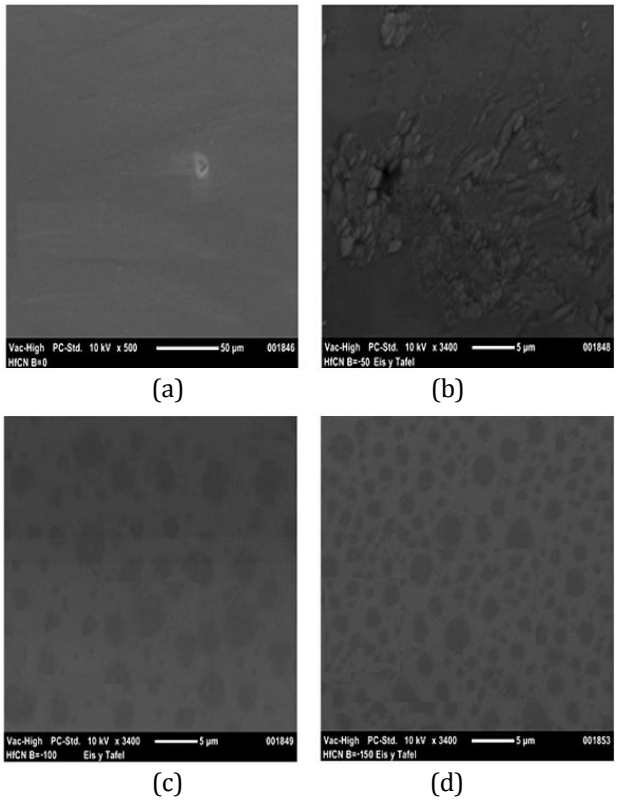

Fig. 9. SEM micrographs for the Hf-C-N/steel (D3) system after the corrosion tests: (a) HfCN coating deposited with 0 V, (b) HfCN coating deposited with -50 V, (c) HfCN coating deposited with -100 V and (d) HfCN coating deposited with -150 V.

So, the changes in the gray scale indicate areas with few corrosion processes, which indicate the homogeneity of the surface coating, demonstrating that this coating can act as a diffusion barrier which protected the steel substrate against the corrosive ions (Cl^-). On the other hand, Figs. 9b-9d show different surface areas for the samples deposited at bias voltage of -50, -100 and -150 V, respectively. From these micrographs it was possible to observe the corrosive attack such as local delamination and pitting corrosion on steel HfCN/steel (D3) system, which indicates an exposition of the steel substrate. Also in the surface analysis for the HfCN coating deposited at -150 V some traces of corrosive solution composed by Cl^- ions was found on the corroded surface (Fig. 9d), which are characteristic of the electrochemical system, due to the adsorption process generated by the diffusion effect. Taking in account the differences on the gray scale from SEM images in Fig. 9 it was possible to estimate the ratio between corroded and non-corroded areas in order to get an idea of the coatings protective ability from microscopic data. Therefore, it is possible to observe that the HfCN coating deposited with a negative bias voltage of 0 V presents the lowest corrosion attack.

3.6 The porosity factor and protective efficiency

The porosity factor values are shown in Fig. 10a, aiming to compare the protective efficiency of HfCN/steel (D3) system as a function of applied negative bias voltage. In this research, the protective efficiency of the coatings was calculated in terms of the polarization resistance. These values are obtained replacing the polarization resistance values on Eq. (2) applied for all HfCN coatings [25].

$$Pf_{Rp} = \frac{R_{p,u}}{R_{p,r-u}} \tag{2}$$

Where P_{fRp}(%) is the porosity factor of HfCN coatings written in terms of polarization resistance, $R_{p,u}$ is the polarization resistance of the uncoated D3 steel and R= is the measured polarization resistance of HfCN coating-substrate system [25-28]. Therefore, the analysis of the porosity factor values (P_{fRp}) applied in all coatings suggests that the porosity factor written in terms of polarization resistance of the HfCN coating deposited at 0 V (0.005 %) is lower than the HfCN coating deposited at negative bias voltage of -150 V (0.045 %). These results are according to homogeneous coating surface observed by SEM results (Fig. 4), and the low values of the corrosion rate (Fig. 7).

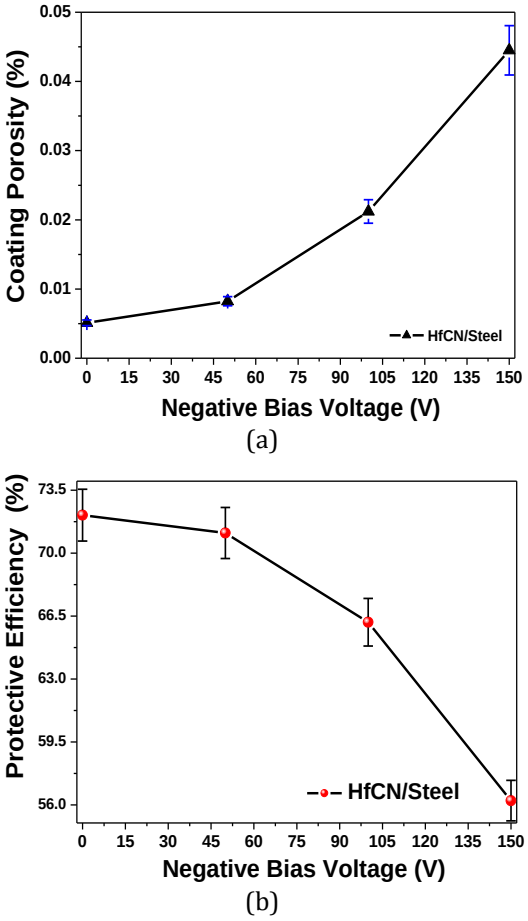

Fig. 10. Electrochemical properties for HfCN coatings: (a) coating porosity factor as function of applied negative bias voltage and (b) protective efficiency factor as a function of applied negative bias voltage.

The protective efficiency of a single HfCN layer was determined by observing the surface nature and taking into account the electrochemical nature (Fig. 10b). Therefore, the protective efficiency factor associated with the different coatings is in agreement with the work reported by Moreno et al. [29]. Thus, the protective efficiency factor corresponds to the ratio of the difference between corrosion intensity of uncoated AISI D3 steel and the corrosion intensity for the same steel coated with HfCN coatings and corrosion intensity of the uncoated AISI D3 steel, which is shown in the following equation (3) [30,31]:

$$Ef\,(\%) = \left(\frac{I_{corr_S} - I_{corr_f}}{I_{corr_S}} \right) \times 100 \qquad (3)$$

Where Ef(%) is the protective efficiency factor, Icorrs is the corrosion intensity of the uncoated steel substrate, and I_{corrf} is the corrosion intensity of the steel substrate coated with HfCN material [27]. The protective efficiency factor values obtained are presented, replacing the electrochemical values on Eq. (3) for all HfCN coatings. The porosity factor is determined for the Hf-C-N coating deposited at 0 V (99.999 %), resulting higher than the Hf-C-N coating deposited at -150 V, (99.989 %), evidencing the best protective nature corresponds to the Hf-C-N coatings material. Moreover, these results are in agreement with SEM results (Fig. 4), and the low values of the corrosion rate (Fig. 8).

3.7 Tribocorrosion Performance

Tribological properties of carbon nitride coatings (HfCN) are provided in Fig. 11 for comparison in relation to single layer systems. These tribological results showed the reduction of the friction coefficient while the applied negative bias is increased. Thus, the friction coefficient of Hf-C-N coatings ranged from approximately 0.36–0.57, being the lowest value reported for the single layers growth with V =150 V (friction coefficient 0.57) [32]. In this regard, the friction coefficient value represented a decrease at approximately 58% of the friction coefficient with respect to the HfCN coating deposited with 0 V. The last behavior can be related to the friction mechanical model proposed by Archard [33], which relates the contribution of the contact surface roughness and the elastic-plastic properties of the coating.

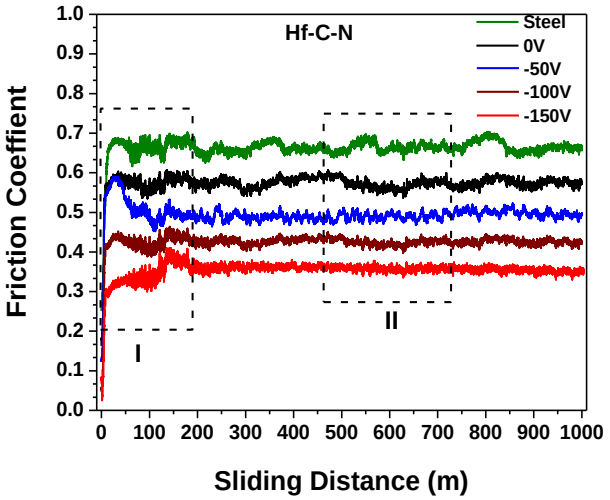

Fig. 11. Tribological results of friction coefficient as a function of sliding distance for D3 steel substrates coated with HfCN coatings as a function of the applied negative bias voltage.

Recent advances in the development of metal-ceramic coatings are summarized and discussed in terms of their relevance to practical

applications. Therefore, it is possible to observe that the elastic strain to failure, which is related to mechanical properties, affects the tribological behavior of Hf-C-N single layer. That provides superior wear resistance when deposited on the substrate materials for mechanical applications [34]. Consequently, this behavior suggests that improving plastic deformation resistance when the negative bias voltage is increased exerts more wear resistance due to enhanced mechanical properties associated with the changes in the internal stress (previously observed in XRD results). Thus, generating a reduction in the friction coefficient as function of negative bias voltage increase is observed (Fig 13).

Table 3. Hardness and Friction coefficient as function of applied negative bias voltages for Hf-C-N coatings.

	Negative Bias Voltage				
Hardness (GPa)	**Steel**	**0V**	**-50V**	**-100V**	**-150V**
		17	24	29	32
Friction coefficient	0.66	0.57	0.49	0.42	0.36

As can be seen in Fig. 12 (SEM micrographs), it is possible to find different wear mechanisms, such abrasive wear (scuffing), adhesive wear, oxidation, and diffusion which are evidenced. In this sense, the abrasion mechanism is a predominant phenomenon at Hf-C-N coatings with low bias voltage (low mechanical and tribological properties, (Table 3 and Fig. 11). The values for negative bias voltage at which the maximum wear values occur will depend on different factors like the combination of low hardness and high friction coefficient, among others. Therefore, in this research work, it has been presented that the wear surfaces for HfCN coatings deposited with different bias voltages (from 0 V to -150 V), show thus changes in the wear mechanisms when the negative bias voltages are applied and increased respectively (e.g reduction in scuffing presence on HfCN deposited with 150 V), in this sense it is possible to observe an increase of wear resistance properties as function of increase of mechanical properties due to the resistance to plastic deformation which are associate to the physical properties observed in, XRD and XPS results.

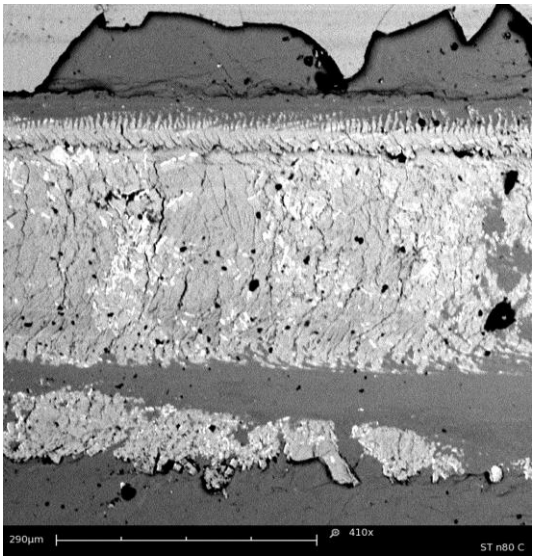

(a)

(b)

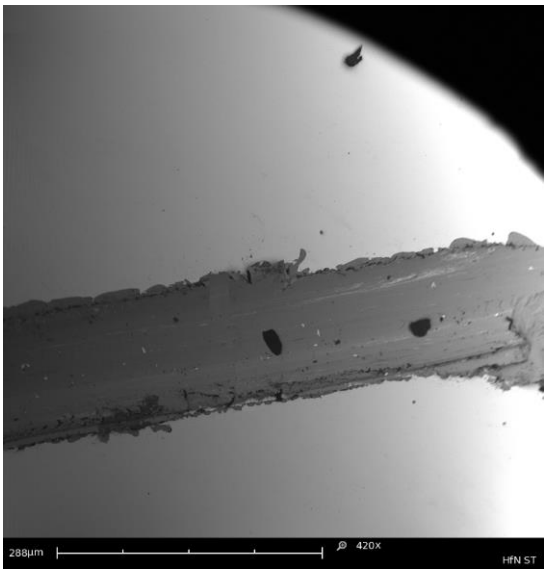

(c)

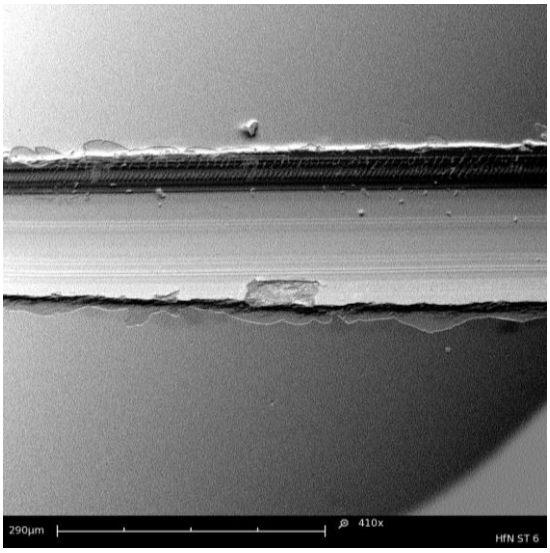

(d)

Fig. 12. SEM micrographs of wear track on Hf-C-N coatings deposited on AISI D3 steel as function of applied negative bias voltage: (a) 0V, (b) -50V, (c) -100V and (d) -150V.

3.7 Adherence analysis by using a critical load criterion

The scratch test was used to characterize the coating adherence strength. The adhesion properties of single-layer coatings can be characterized by the following two terms: L_{C1}, the lower critical load, which is defined as the load where cracks first occurred (cohesive failure); and L_{C2}, the upper critical load, which is the load where the first delaminating at the edge of the scratch track occurred (adhesive failure) The values of critical load (L_{C1} and L_{C2}) for the different coatings are shown in Fig. 13.

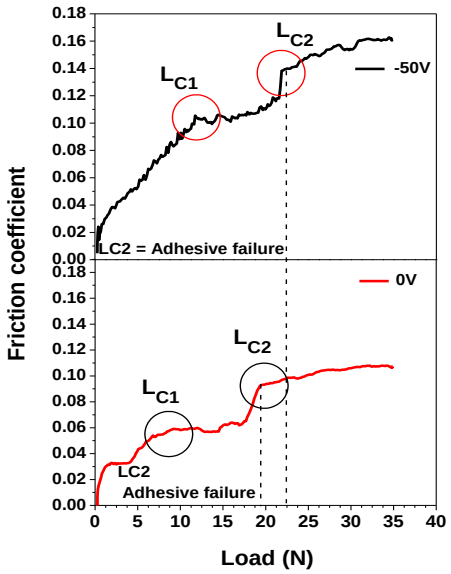

(a)

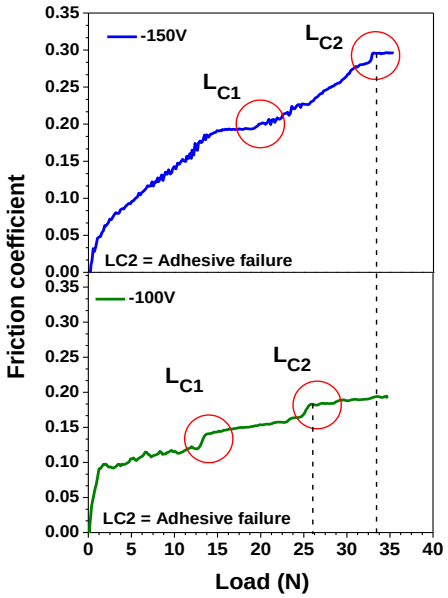

(b)

Fig. 13. Tribological results for friction coefficient curves vs. applied load for Hf-C-N coatings deposited with different applied negative bias voltages, showing thus the adhesion failure (L_{C2}): (a) 0 V and -50 V, (b) -100 V and -150 V.

The L_{C1} was shown for the different coatings in the range of 7-18 N, in which the lowest value was attributed to the hard coatings deposited with bias voltage of 0V and the highest value was attributed to the Hf-C-N ternary system growth with negative bias voltage of -150 V. So analyzing the adhesive critical loads values (L_{C2}) from 18 N to 34 N is possible to observed that the critical load increase when the negative bias voltage increaser due to the improvements in the mechanical properties.

3.9 Correlation between tribological and electrochemical properties

Figure 14 shows the relationship between negative bias voltage, hardness and polarization resistance for Hf-C-N coatings. In Fig. 14 it is clearly shown that the reduction of friction coefficient by increase of hardness (Table 3), when the negative bias voltage increases, is associated with a increasing of the corrosion rate, due to the increase of porosity factor (Fig. 10a) and decrease the protective efficiency factor (Fig. 10b), produced by Ar^{+}-ion bombardment at higher bias voltages. From this correlation it is possible to determine that one merit index [35] associates to an acceptable friction coefficient and corrosion rate at the same negative bias voltage.

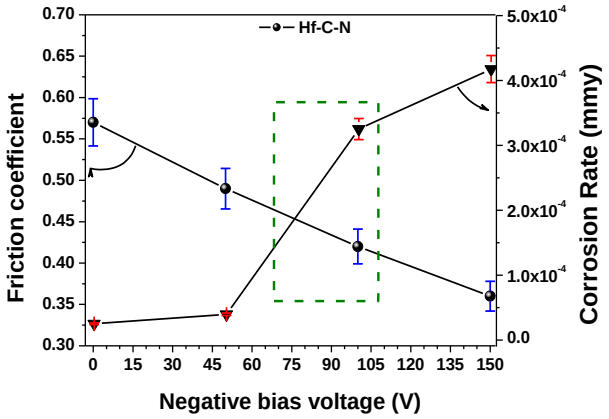

Fig. 14. Correlation between mechanical and electrochemical properties of Hf-C–N films deposited at different applied negative bias voltage.

Therefore, the Hf-C-N coatings deposited around −100 V offer the best synergy for mechanical and electrochemical properties with good hardness and an acceptable polarization resistance and corrosion rate.

4. CONCLUSIONS

The Hf-C-N like ternary coatings were successfully deposited by r.f. magnetron sputtering. The XRD analysis showed that the coatings were highly crystalline. From XPS results it was possible to identify the chemical composition in all ternary materials as a function of negative bias voltage (from Hf-C-N 0V to Hf-C-N-150V).

The surface morphologies of the samples were determined via SEM, establishing thus a homogeneous surface for all Hf-C-N coatings after electrochemical processes. The electrochemical behavior was studied, observing changes for all coatings in the polarization resistances and corrosion rates as a function of applied negative bias voltage. It was also shown that the polarization resistance and the corrosion rate, decreases and increases, respectively, as the negative bias voltage was increased.

The corrosive effects and tribological properties in the coatings can be attributed to the higher ion bombardment generated by the high bias voltages. The samples deposited at high bias voltages can generate micro-cracks, as corroborated by SEM and the porosity factor analysis. The latter finding suggests that the porosity factor increases with bias voltage together with the reduction of protective efficiency coatings values.

The merit index found in this work suggests that HfCN coating deposited at a bias of −100 V offers the best synergy for tribological and electrochemical properties which can be applied in industrial devices that requires high performance.

Acknowledgements

Dr Willian Aperador thanks the "Vicerrectoría de Investigaciones de la Universidad Militar Nueva Granada" project number ING-2630, validity 2018.

Author Contributions: Willian Aperador performed the obtaining coatings; Will Piedrahita worked in measurements in SEM, XPS and XRD and performed the interpretation of the data and the respective analysis. Julio Caicedo performed measurements corrosion tests performed the interpretation of the data.

REFERENCES

[1] Y.S. Yang, T.P. Cho, H.W. Ye, *The effect of deposition parameters on the mechanical properties of Cr-C-N coatings*, Surface and Coatings Technology, vol. 259, pp. 141-145, 2014, doi: 10.1016/j.surfcoat.2014.02.035

[2] F. Zhou, K. Adachi, K. Kato, *Friction and wear behavior of BCN coatings sliding against ceramic and steel balls in various environments*, Wear, vol. 261, iss. 3-4, pp. 301-310, 2006, doi: 10.1016/j.wear.2005.10.009

[3] J.C. Caicedo, C. Amaya, L. Yate, W. Aperador, G. Zambrano, M.E. Gómez, J. Alvarado-Rivera, J. Muñoz-Saldaña, P. Prieto, *Effect of applied bias voltage on corrosion-resistance for TiC1-xNx and Ti1-xNbxC1-yNy coatings*, Applied Surface Science, vol. 256, iss. 9, pp. 2876-2883, 2010, doi: 10.1016/j.apsusc.2009.11.042

[4] E. Grigore, C. Ruset, C. Luculescu, *The structure and properties of VN-VCN-VC coatings deposited by a high energy ion assisted magnetron sputtering method*, Surface and Coatings Technology, vol. 205, pp. S29-S32, 2011, doi: 10.1016/j.surfcoat.2011.03.023

[5] J.C. Caicedo C. Amaya, L. Yate, M.E. Gómez, G. Zambrano, J. Alvarado-Rivera, J. Muñoz-Saldaña, P. Prieto, *TiCN/TiNbCN multilayer coatings with enhanced mechanical properties*, Applied Surface

Science, vol. 256, iss. 20, pp. 5898-5904, 2010, doi: 10.1016/j.apsusc.2010.03.071

[6] C. Mitterer, N. Fateh, F. Munnik, *Microstructure–property relations of reactively magnetron sputtered VCxNy films*, Surface and Coatings Technology, vol. 205, iss. 13-14, pp. 3805-3809, 2011, doi: 10.1016/j.surfcoat.2011.01.037

[7] C.M. Cotruta, V. Braicb, M. Balaceanub, I. Titorencuc, M. Braicb, A.C. Paraua, *Corrosion resistance, mechanical properties and biocompatibility of Hf-containing ZrCN coatings*, Thin Solid Films, vol. 538, pp. 48-55, 2013, doi: 10.1016/j.tsf.2012.12.100

[8] E. Lewin, P.O.A. Persson, M. Lattemann, M. Stuber, M. Gorgoi, A. Sandell, C. Ziebert, F. Schafers, W. Braun, J. Halbritter, S. Ulrich, W. Eberhardt, L. Hultman, H. Siegbahn, S. Svensson, U. Jansson, *On the origin of a third spectral component of C1s XPS-spectra for nc-TiC/a-C nanocomposite thin films*, Surface Coatings Technology, vol. 202, iss. 15, pp. 3563-3570, 2008, doi: 10.1016/j.surfcoat.2007.12.038

[9] M.D. Antonik, R.J. Lad, T.M. Christensen, *Clean Surface and Oxidation Behavior of Vanadium Carbide*, VC0.75(100), Surface and Interface Analysis, vol. 24, iss. 10, pp. 681-686, 1996.

[10] E. Ech-Chamikh, A. Essafti, Y. Ijdiyaou, M. Azizan, *XPS study of amorphous carbon nitride (a-C:N) thin films deposited by reactive RF sputtering*, Solar Energy Materials and Solar Cells, vol. 90, iss. 10, pp. 1420-1423, 2006, doi: 10.1016/j.solmat.2005.10.007

[11] G. Kamath, A.P. Ehiasarian, Y. Purandare, P.Eh. Hovsepian, *Tribological and oxidation behaviour of TiAlCN/VCN nanoscale multilayer coating deposited by the combined HIPIMS/(HIPIMS-UBM) technique*, Surface and Coatings Technology, vol. 205, iss. 8-9, pp. 2823-2829, 2011, doi: 10.1016/j.surfcoat.2010.10.049

[12] L. Ramqvist, K. Hamrin, G. Johansson, A. Fahlman, C. Nordling, *Charge transfer in transition metal carbides and related compounds studied by ESCA*, Journal of Physics and Chemistry of Solids, vol. 30, iss. 7, pp. 1835-1847, 1969, doi: 10.1016/0022-3697(69)90252-2

[13] N. Fateh, G.A. Fontalvo, G. Gassner, C. Mitterer, *Influence of high-temperature oxide formation on the tribological behaviour of TiN and VN coatings*, Wear, vol. 262, iss. 9-10, pp. 1152-1158, 2007, doi: 10.1016/j.wear.2006.11.006

[14] G. Gonçalves, M. Vila, I. Bdikin, A. Andrés, N. Emami, R.A.S. Ferreira, L.D. Carlos, J. Grácio, P.A. A.P. Marques, *Breakdown into nanoscale of graphene oxide: Confined hot spot atomic reduction and fragmentation*, Scientific Reports, vol. 4, pp. 6735-6748, 2014, doi: 10.1038/srep06735

[15] J. Li, X. Liu, C. Cao, J. Guo, Z. Pan, *Silica-gel Supported V Complexes: Preparation, Characterization and Catalytic Oxidative Desulfurization*, Chinese Journal of Chemical Engineering, vol. 21, iss. 8, pp. 860-866, 2013, doi: 10.1016/S1004-9541(13)60558-3

[16] M. Bacal, J. Perrière, M. Tanguy, A.N. Vesselovzorov, K.I. Maslakov, A.P. Dementjev, *Study of carbon nitride films deposited using a Hall-type ion source*, Journal of Physics D: Applied Physics, vol. 33, pp. 2373-2385, 2000, doi: 10.1088/0022-3727/33/19/305

[17] R. Franz, J. Neidhard, B. Sartory, R. Tessadri, C. Mitterer, *Micro- and bonding structure of arc-evaporated AlCrVN hard coatings*, Thin Solid Films, vol. 516, iss. 18, pp. 6151-6157, 2008, doi: 10.1016/j.tsf.2007.11.024

[18] E. Grigore, C. Ruset, C. Luculescu, *The structure and properties of VN-VCN-VC coatings deposited by a high energy ion assisted magnetron sputtering method*, Surface and Coatings Technology, vol. 205, pp. 29-32, 2011, doi: 10.1016/j.surfcoat.2011.03.023

[19] I. Carvalho, M. Henriques, J.C. Oliveira, C.F.A. Alves, A.P. Piedade, S. Carvalho, *Influence of surface features on the adhesion of Staphylococcus epidermidis to Ag–TiCN thin films*, Science and Technology of Advanced Materials, vol. 14, iss. 3, pp. 1-9, 2013, doi: 10.1088/1468-6996/14/3/035009

[20] R. Giovanardi, R. Sola, P. Veronesi, G. Poli, P. Veronesi, *Corrosion resistance improvement of nitrocarburised and post-oxidised steels by oil impregnation*, Corrosion Engineering, Science and Technology, vol 47, iss 2. pp. 107-115, 2012, doi: 10.1179/1743278211Y.0000000027

[21] J.E.B. Randles, *Kinetics of rapid electrode reactions*, Discussions of the Faraday Society, vol. 1, pp. 11-18, 1947, doi: 10.1039/DF9470100011

[22] L.F. Sennaa, C.A. Achete, R.A. Simão, T. Hirsch, *Comparative Study between the Electrochemical Behavior of TiN, TiCxNy and CrN Hard Coatings by Using Microscopy and Electrochemical Techniques*, Materials Research, vol 4, no. 2, pp. 137-141, 2001, doi: 10.1590/S1516-14392001000200017

[23] R. Sola, G. Poli, P. Veronesi, R. Giovanardi, *Effects of surface morphology on the wear and corrosion resistance of post-treated Nitrided and nitrocarburized 42CrMo4 steel*, Metallurgical and Materials Transactions A: Physical Metallurgy and Materials Science, vol. 45, iss. 6, pp. 2827-2833, 2014, doi: 10.1007/s11661-014-2219-z

[24] R. Sola, *Post-treatment surface morphology effect on the wear and corrosion resistance of nitrided and nitrocarburized 41 CrAlMo7 steel*, La Metallurgia Italiana, vol. 102, pp. 21-31, 2010.

[25] N. Madaoui, N. Saoula, B. Zaidc, D. Saidic, A.Si. Ahmed, *Structural, mechanical and electrochemical comparison of TiN and TiCN coatings on XC48 steel substrates in NaCl 3.5% water solution*, Applied Surface Science, vol. 312, pp. 134-138, 2014, doi: 10.1016/j.apsusc.2014.04.167

[26] W. Tato, D. Landolt, *Electrochemical Determination of the Porosity of Single and Duplex PVD Coatings of Titanium and Titanium Nitride on Brass*, Journal of The Electrochemical Society, vol. 145, iss. 12, 4173-4184, 1998, doi: 10.1149/1.1838932

[27] K. Chang, S. Chung, Lai, H. Shih, *The electrochemical behavior of thermally oxidized CrN coatings deposited on steel by cathodic arc plasma deposition*, Applied Surface Science, vol. 236, iss. 1-4, pp. 406-415, 2004, doi: 10.1016/j.apsusc.2004.05.024

[28] H. Altun, S. Sen, *The effect of DC magnetron sputtering AlN coatings on the corrosion behaviour of magnesium alloys*, Surface and Coatings Technology, vol. 197, pp. 193-200, 2005, doi: 10.1016/j.surfcoat.2004.06.001

[29] C. Moreno, S. Hernández, J.J. Santana, J. González Guzmán, R.M. Souto, S. González, *Characterization of Water Uptake by Organic Coatings Used for the Corrosion Protection of steel as Determined from Capacitance Measurements*, International journal of electrochemical science, vol. 7, pp. 7390-7403, 2012.

[30] Y.H. Yoo, D.P. Le, J.G. Kim, S.K. Kim, and P.V. Vinh, *Corrosion Behavior of TiN, TiAlN, TiAlSiN Thin Films Deposited on Tool Steel in the 3.5 wt.% NaCl Solution*, Thin Solid Films, vol. 516, iss. 11, pp. 3544–3548, 2008, doi: 10.1016/j.tsf.2007.08.069

[31] R. Sola, R. Giovanardi, P. Veronesi, G. Parigi, *A novel method for fracture toughness evaluation of tool steels with post-tempering cryogenic treatment*, Metals, vol. 7, pp. 1-9, 2017, doi: 10.3390/met7030075

[32] W.C. Oliver, G.M. Pharr, *An improved technique for determining hardness and elastic modulus using load and displacement sensing indentation experiments*, Journal of Materials Research, vol. 7, iss. 6, pp. 1564-1583, 1992, doi: 10.1557/JMR.1992.1564

[33] J.F. Archard, *Contact and rubbing of flat surfaces, Journal of Applied Physics*, vol. 24, iss. 8, pp. 981-992, 1953, doi: 10.1063/1.1721448

[34] A. Leyland, A. Matthews, *On the significance of the H/E ratio in wear control: a nanocomposite coating approach to optimised tribological behavior*, Wear, vol. 246, iss. 1-2, pp. 1-11, 2000, doi: 10.1016/S0043-1648(00)00488-9

[35] J.C. Caicedo, G. Zambrano, W. Aperador, L. Escobar-Alarcon, E. Camps, *Mechanical and electrochemical characterization of vanadium nitride (VN) thin films*, Applied Surface Science, vol. 258, iss. 1, pp. 312-320, 2011, doi: 10.1016/j.apsusc.2011.08.057